TASK QUARTERLY 2 No 2 (1998), 357-372

NUMERICAL STUDY OF THE PARALLEL VORTEX AIRFOIL INTERACTION

JANUSZ PIECHNA AND ANDRZEJ SZUMOWSKI

Faculty of Power and Aeronautical Engineering
Warsaw University of Technology,
Nowowiejska 24, 00-665 Warsaw, Poland

Abstract: The effect of a strong vortex interacting with an airfoil flow is investigated numerically. The finite volume method for Euler equations is applied. Instantanous flow patterns, including pressure distributions along the airfoil and lift coefficients, were calculated for various miss distancees of the vortex passing parallely to the airfoil plane. It has been found that the effects of interaction are much stronger when the vortex approaching the airfoil accelerates the flow at the pressure surface than in the case when the vortex decelerates the flow at the suction surface. The lift coefficient only slightly depends on the vortex core radius if the velocity induced at the airfoil surface by vortices of various cores is constant. In contrast to this the intensity of the acoustic disturbance produced during the interaction strongly depends on the core radius even for a constant induced flow velocity.

1. Introduction

In certain cases of helicopter flight, eg. descent with deep turns or low powered approach to landing, the rotor blade tip vortices strongly disturb the flow at the following blades. As a result, the blade loading considerably varies. This leads to vibrations of the blade and of the remaining elements of the helicopter structure. The variations of blade loading are accompanied by impulsive noise with high intensity.

The strongest effects of the airfoil-vortex interaction (AVI) occur when the vortex passes parallel and close to the airfoil plane. This was the main reason why the majority of the investigators who studied the AVI phenomenon considered two-dimensional model of interaction.

The vortex filament can pass at various miss distances along both the upper and bottom surfaces of the airfoil. When it is equal to zero a head-on impact occurs. This problem was investigated by Lee and Bershader [1, 2]. They solved the Navier-Stokes equations using a fifth order upwind scheme based on Osher-type of flux differencing. The isolines of density calculated by the above authors qualitatively coincide with those observed in the corresponding interferometric photographs. The sound wave which appears due to an expansion of high pressure

air in the stagnation region was also predicted in the papers mentioned above (pressure in the stagnation region increases when the vortex approaches the leading edge).

Variations of the surface pressure during the AVI for the vortex passing under the airfoil plane (increasing the flow velocity along the bottom surface of the airfoil) were calculated by Damodaran and Caughey [3], Ehrenfried [4] and Gallman [5]. The unsteady Euler equations [3, 4] or full-potential equation for transonic flow [5]were solved. Damodaran and Caughey [3] and Ehrienfried [4] noted a strong influence of the vortex on the lift and pitching moment coefficients. Unfortunately, only one value of the miss distance, equal to a quarter of chord lengh, was considered by the above authors.

The parallel airfoil-vortex interaction is controlled, first of all, by the following parameters:

a) miss distance which is defined as a distance measured at infinity between the vortex trajectory and the stream line passing through the leading edge,

b) vortex strength (radius of vortex core and circulation)

c) angle of attack of the airfoil, and

d) flow Mach number at infinity.

The goal of the present work is to investigate the effect of the first and the second of the four parameters mentioned above. Numerical investigations conducted in the present paper are based on the Euler equations. An axisymmetric clock-wise rotating vortex moving parallely to the NACA 0012 airfoil symmetry plane and interacting with it is taken into account. A constant flow Mach number in the infinity $M_\infty = 0.69$ is assumed.

2. Equations

A coherent vortex of relatively small core which is the subject of the present calculations causes rapid changes of actual flow properties during its passage along the airfoil. It can be assumed that these changes are controlled, first of all, by inertia effects but not by viscous ones.

By this assumption the Euler equations seem adequate for these calculations. The two-dimensional Euler equations in integral form are as follows:

$$\frac{\partial}{\partial t}\int_S U ds + \int_L F dy + \int_L G dx = 0 \ , \tag{1}$$

where

$$U = \begin{pmatrix} \rho \\ \rho u \\ \rho v \\ e \end{pmatrix} \quad F = \begin{pmatrix} \rho u \\ \rho u^2 + p \\ \rho uv \\ (e + p)u \end{pmatrix} \quad G = \begin{pmatrix} \rho v \\ \rho uv \\ \rho v^2 + p \\ (e + p)v \end{pmatrix}$$

$$e = \rho \frac{(u^2 + v^2)}{2} + p/(\gamma - 1)$$

The first integral is related to the control area S and the remaining ones to the control circuit L (encircling the control area).

3. Boundary and Initial Conditions

The calculations performed in the present work correspond to experimental investigations of the AVI process with the use of shock tubes. To reproduce the experimental conditions a control area shown in Figure 1 is considered. Its upper and bottom surfaces correspond to the shock tube walls. Hence, the fluxes across these walls are assumed to be zero. The remaining surfaces represent the cross-sections of the shock tube located upstream and downstream of the test airfoil. For these surfaces a one-dimensional Riemann flow is considered.

For the initial conditions it is assumed that the shock wave running in motionless air reaches the leading edge of the airfoil. The shock wave is followed by an axisymmetric vortex convected in a uniform flow. The vortex center in the initial

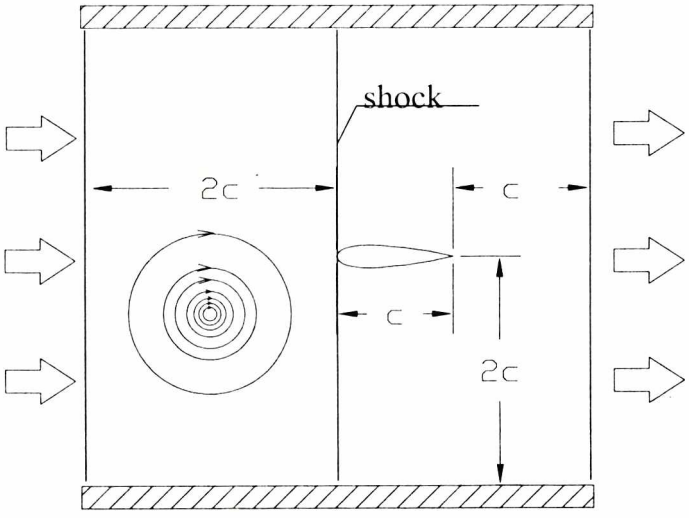

Figure 1 *Control area, c=120 mm*

phase of computation is located half a distance between the shock front and the upstream control surface. It is assumed that the flow velocity induced by the vortex at the upper and bottom walls, as well as at the upstream cross-section and at the shock front is small enough to be neglected. For the vortex considered (see below) it is under 5% of the flow velocity behind the shock wave. The calculations were stopped when the vortex leaves the trailing edge of the airfoil.

The flow velocity induced by the vortex for the initial phase of interaction is obtained from the following relationship

$$V_\theta = \frac{\Gamma_0}{2\pi r} \frac{r^2(2+\alpha)}{r^2 \exp(\alpha(r-r_0)/r_0) + (1+\alpha)r_0^2}, \tag{2}$$

where:

V_θ — tangential velocity,
r_0 — vortex core radius,
Γ_0 — circulation at $r = r_0$,
α — coefficient controlling velocity distribution.

The coefficient strongly influences the velocity distribution outside the vortex

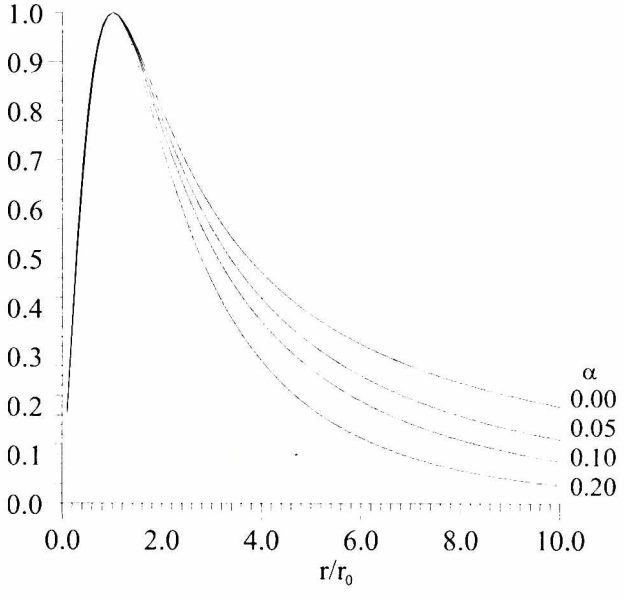

Figure 2. *Velocity distributions in the vortex*

core but weakly inside it (Figure 2).

For the experimental data which can be found in Refs [6] $\alpha = 0.15$. For this α the velocity decay (in the radial direction) in the vortex is much stronger than for the classical vortex model with $\alpha = 0$ (see Figure 2). Taking into account this feature, one can consider a smaller control volume for $\alpha > 0$ than in the case of the classical vortex. The pressure distribution corresponding to $V_0(r)$ can be found using

the momentum

$$\frac{dp}{dr} = \frac{\rho V_\theta^2}{r}, \tag{3}$$

and energy equation for adiabatic flow:

$$\frac{\gamma}{\gamma - 1}\frac{p}{\rho} + \frac{V_\theta^2}{2} = \frac{\gamma}{\gamma - 1}\frac{p_\infty}{\rho_\infty}, \tag{4}$$

where p_∞ and ρ_∞ mean the pressure and density far from the vortex core, respectively.

The parameters Γ_0, r_0 and α in Eq. (1) can be chosen to match the real pressure distribution in the vortex. To obtain these parameters the pressure in the vortex center, the maximum of pressure derivative $(dp/dr)_{\max}$ and the radius corresponding to $(dp/dr)_{\max}$ determined from the measured function $p(r)$ can be used. The appropriate procedure is presented in Ref. [6]. In the present calculations the following values for Γ_0, r_0/c and α were assumed 50 m²/s, 0.045, 0.15, respectively for the reference case.

4. Numerical Procedure

The finite volume method is used. Eq. (1) for a cell j of finite area ΔS yields:

$$\frac{dU_j}{dt} = \frac{1}{\Delta S}\sum\left(F\,\Delta y + G\,\Delta x\right). \tag{5}$$

In the case of a quadrilateral cell (Figure 3) the right hand side of the above equation is:

$$\begin{aligned}\frac{1}{\Delta S}\Big\{&-\left(F_{i+1/2,j}\right)\left(y_P - y_Q\right)+\left(G_{i+1/2,j}\right)\left(x_P - x_Q\right)+\\&-\left(F_{i-1/2,j}\right)\left(y_R - y_S\right)-\left(G_{i-1/2,j}\right)\left(x_R - x_S\right)+\\&-\left(F_{i,j+1/2}\right)\left(y_S - y_P\right)+\left(G_{i,j+1/2}\right)\left(x_S - x_P\right)+\\&-\left(F_{i,j-1/2}\right)\left(y_Q - y_R\right)+\left(G_{i,j-1/2}\right)\left(x_Q - x_R\right)\Big\}\end{aligned}$$

Each flux vector shown in Figure 3 is composed of two terms, e.g.

$$F_{i+1/2,j} = F^+_{i,j} + F^-_{i+1,j}\,. \tag{6}$$

The first and the second term on the right hand side are the forward and the backward contributions of the fluxes produced by the neighbouring cells i, j and $i+1, j$, respectively (Figure 4).

The contributions are obtained by splitting the flux vector F, in the way proposed

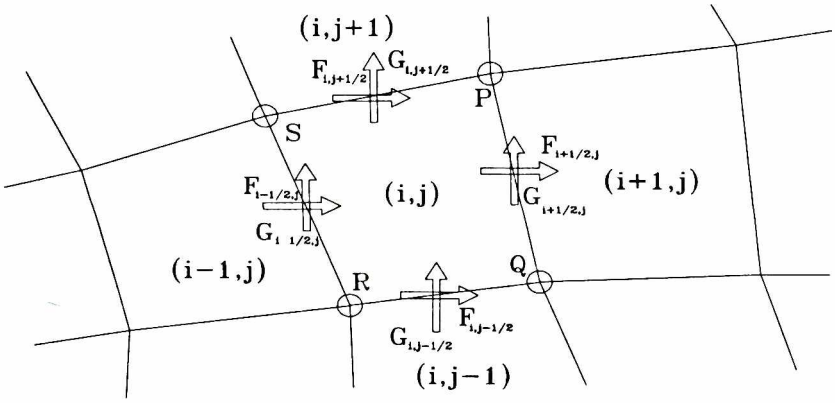

Figure 3. *Notation of the fluxes*

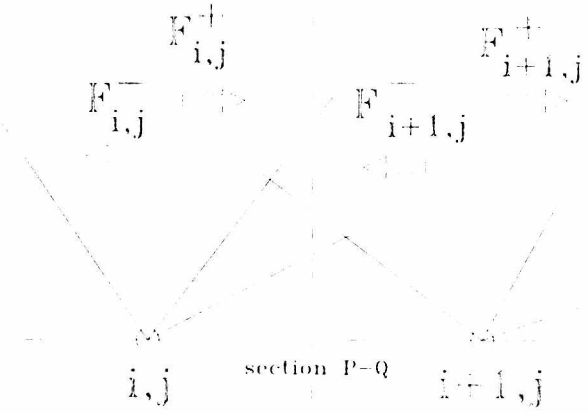

Figure 4. *Flux splitting*

by van Leer [7], as follows:
for $-a < u < a$ (a means the speed of sound)

$$F^{\pm} = \begin{Bmatrix} f^{\pm} \\ f^{\pm}\left[(\gamma-1)u \pm 2a\right]/\gamma \\ f^{\pm}v \\ f^{\pm}\left\{\left[(\gamma-1)u \pm 2a\right]/\left[2\left(\gamma^2-1\right)\right] + v^2/2\right\} \end{Bmatrix},$$

where:

$$f^{\pm} = \rho\left(u+a\right)^2/\left(4a\right),$$

for $u > a$

$$F^{+} = F, \quad F^{-} = 0,$$

and for $u > -a$

$$F^+ = 0, \quad F^- = F.$$

The second order Runge-Kutta procedure was applied to integrate eq (5).

Almost 360 000 cells uniformly distributed in the control volume were used. Such a large number of cells was chosen to prevent numerical dispersion of the vortex during its passage.

5. Results

5. 1 Effect of vortex trajectory

Figures 5a-f show the pressure isolines for three phases of the AVI process. The vortex was initially positioned under (at h/c = –0.2) or over (h/c = 0.2) the airfoil symmetry plane for the figures in the first and the second column, respectively. In figures 5a and 5d one can see the clockwise rotating vortex approaching the airfoil.

The vortex disturbs the bow shock wave which appears when the incident shock wave reflects at the leading section of the airfoil. Due to the vortex, the stagnation point leaves its initial position at the leading edge and shifts on to the upper surface independently of the vortex initial location (h/c = –0.2 and 0.2). However, when the vortex reaches the region very close to the leading edge, the flow patterns become strongly dependent on the vortex trajectory, i.e. on weather the vortex passes over or under the airfoil. In the former case the stagnation point moves onto in the bottom surface of the airfoil. It comes back again to the leading edge after some delay (Figure 5e) as the vortex is being convected.

In contrast to this, the latter case exhibits much stronger variations of the flow pattern. The vortex, when it passes the leading edge (Figure 5b), induces a supersonic flow region at the bottom surface of the airfoil. In this region there is a shock wave. Simultaneously, a strong disturbance (compressibility wave) is created at the leading section of the airfoil. It appears due to the expansion of the air in the stagnation region as the vortex passes the leading edge (the air in the stagnation region was initially compressed to high pressure owing to high velocity induced by the vortex). The compressibility wave which expands in the space under the airfoil is visible in Figure 5c. The bow shocks visible in this figure at both the upper and the bottom surfaces form due to steepening of the compressibility waves.

The pressure distributions along the upper and bottom surfaces of the airfoil, corresponding to instantaneous flow patterns described above, are shown in Figures 6a-c. They are compared with those for the flow without vortex. For the phase of interaction shown in Figure 6a, for which the vortex only weakly influences the airfoil flow, the pressure distributions along upper and bottom surfaces are very close to those obtained for the case without the vortex. The difference between the pressure distributions increases as the vortex approaches the leading edge. In the phase shown in Figure 6b the supersonic flow region divided into two parts by a shock wave can be noted at the bottom surface. This suggests that the shock in

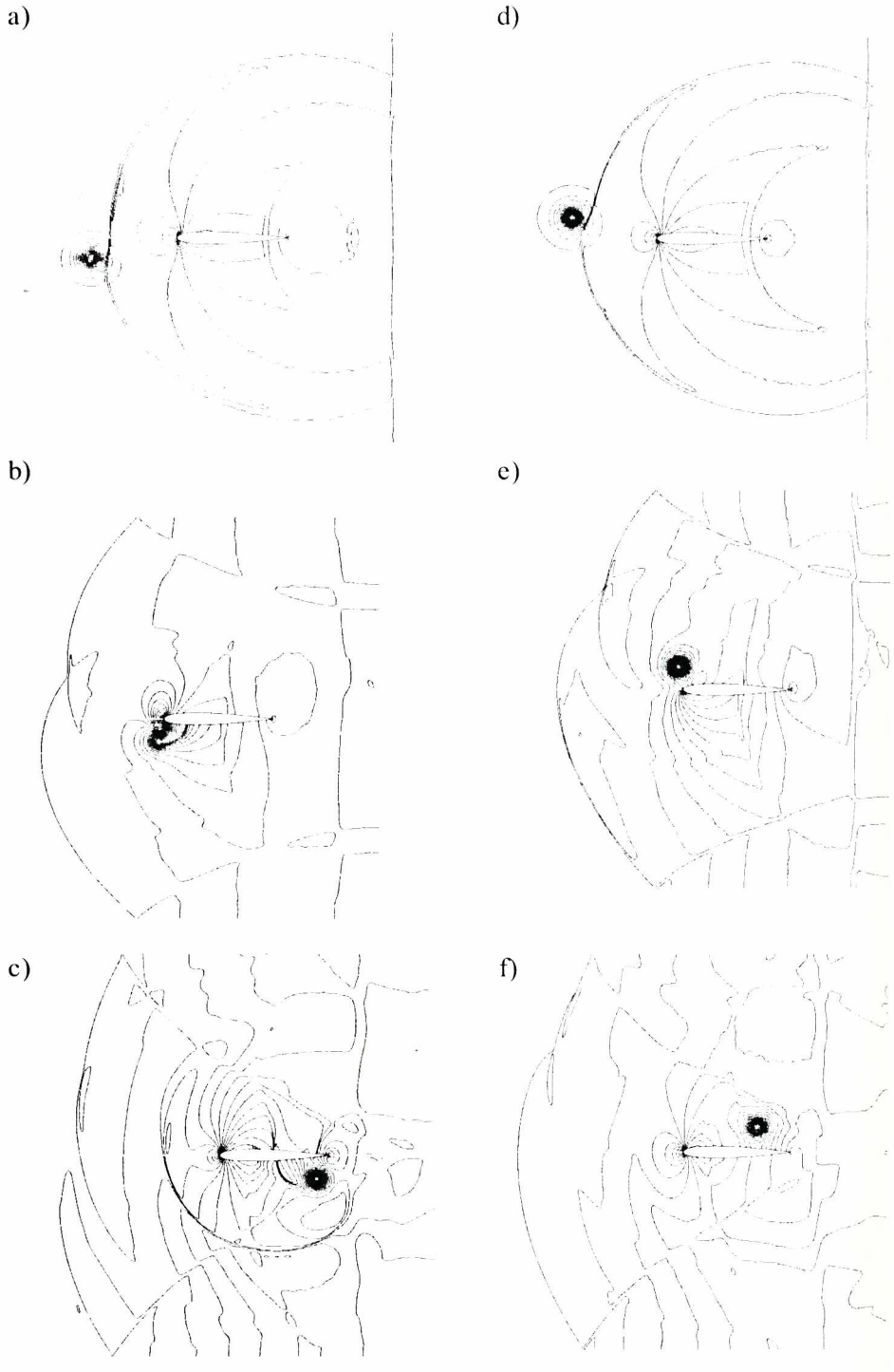

Figure 5. *Instantanous pressure isolines for the vortex passing under (first column) and over (second column) the airfoil. Delay in relation to the moment when the incident shock wave reaches the leading edge: (a, b) 0. 508 ms, (b, e) 0. 848 ms, (c, f) 1. 186 ms.*

a)

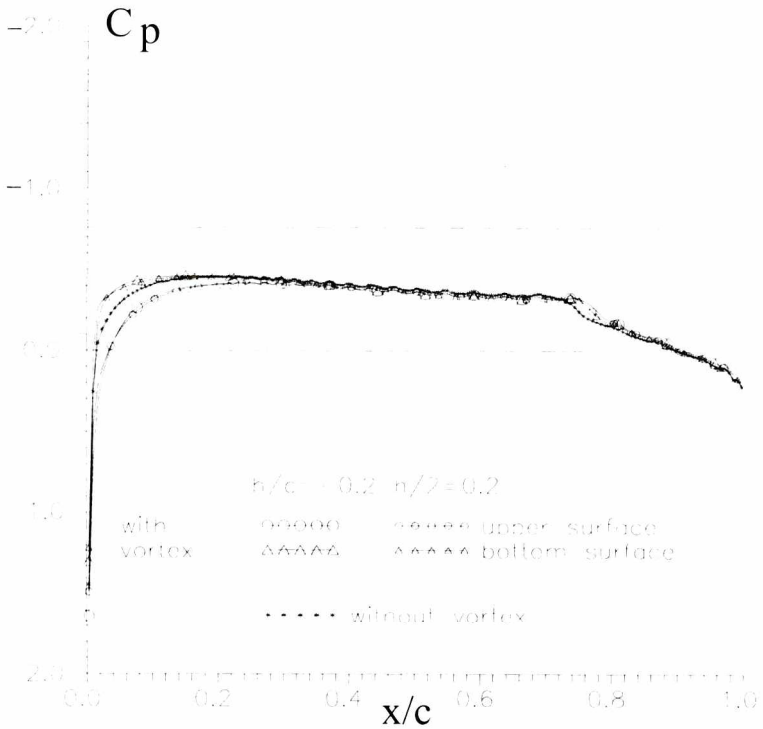
Cp
h/c = 0.2 n/2=0.2
with vortex
upper surface
bottom surface
without vortex
x/c

b)

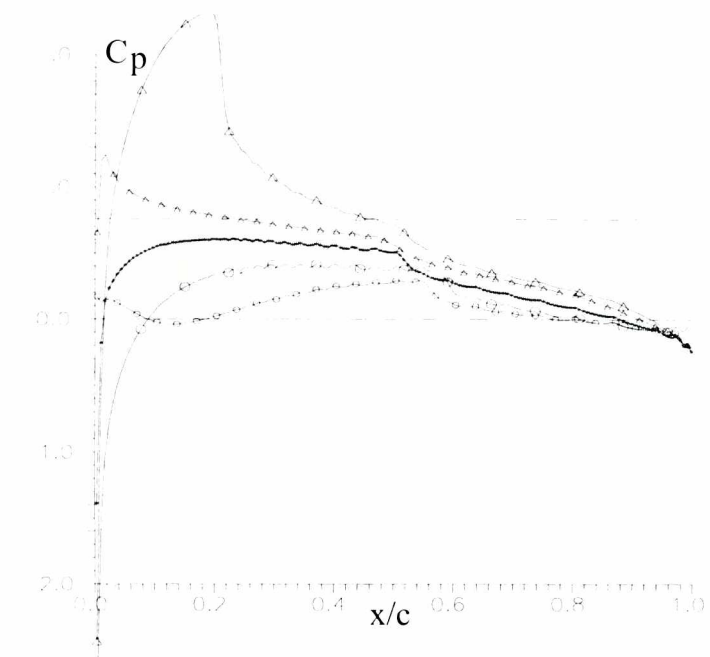
Cp
x/c

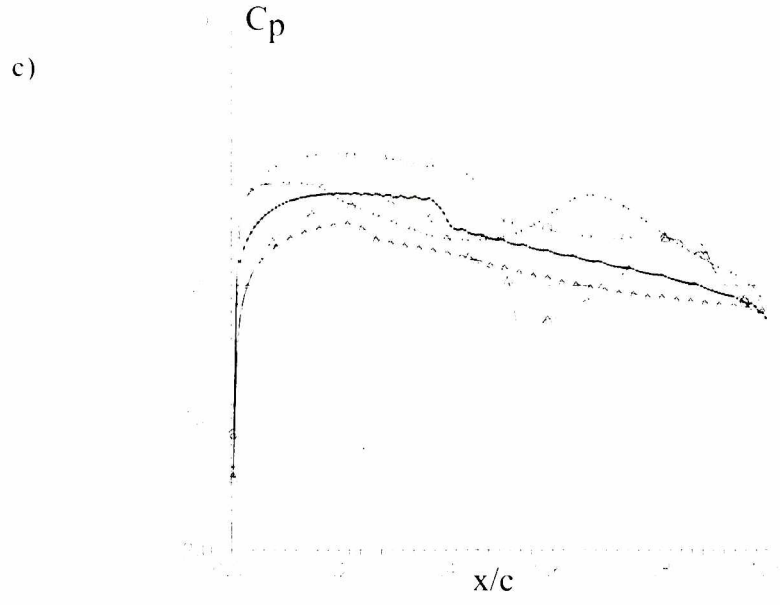

Figure 6. *Instantanous surface pressure coefficient (Cp) distributions corresponding to flow patterns shown in Figure 5. Dashed line means sonic flow*

this phase moves upstream and is followed by a compressibility wave. One can see that for the initial phases of the AVI, when the vortex passes the leading section, the average pressure at the bottom surface $(\overline{p}_b)$ is lower than that at the upper surface $(\overline{p}_u)$. The relationship between $\overline{p}_u$ and changes as the vortex passes the airfoil $\overline{p}_b$, increases whereas decreases.

Eventually, for the vortex at the trailing edge, we have $\overline{p}_u < \overline{p}_b$. Variations of pressure do not disappear when the vortex leaves the airfoil. The experiments conducted in Ref. [8] prove that they exist during a relatively long time afterwards.

Analogous behaviour of the surface pressure can also be found for the vortex passing over the airfoil. In this case, however, the pressure variations are much weaker than for the vortex passing under the airfoil at the same miss distance.

Histories of the lift coefficient (C_l) for four values of the miss distance of the vortex passing under the airfoil are presented in Figure 7. It can be noted that variations of C_l show cosine like character. Its amplitude decreases with increasing miss distance. Figure 8 shows a comparison of C_l for two vortex trajectories h/c = 0.2 and h/c = –0.2. It is visible that the amplitude of C_l is larger for negative miss distance.

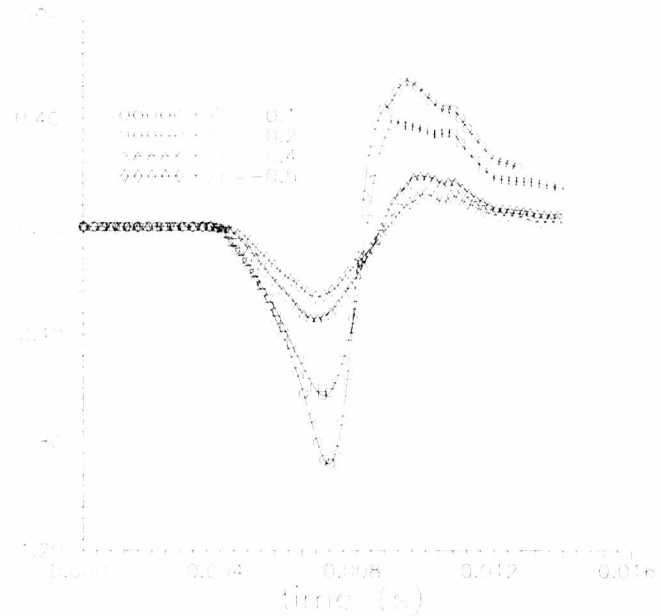

Figure 7. *Lift coefficients for various trajectories*

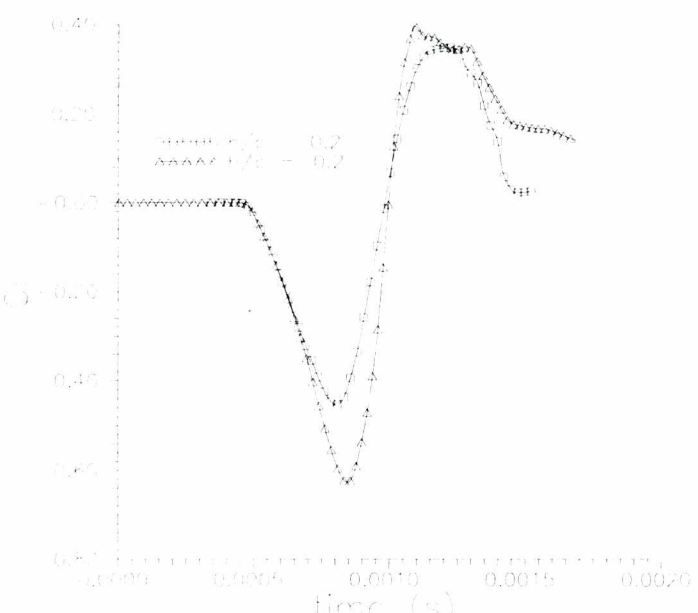

Figure 8. *Lift coefficients for the vortex of the vortex passing under the airfoil passing over (h/c = 0.2) and under (h/c = –0.2) the airfoil*

5.2 Effect of vortex strength

By maintaining constant Γ_0 and α, the value of r_o/c was changed to investigate the effect of the vortex strength (relative core radius) on the airfoil flow behavior. Figure 9 shows the distributions of the flow velocity in the vortex obtained from Eq. (1) for four values of core radius.

Figure 10 presents the instantaneous pressure isolines for two phases of the airfoil-vortex interaction. Figures in the columns on the left and the right hand side correspond to various core radii of the vortex; the core radii for the right hand side column is three times larger than for the left one. In both cases the center of the clockwise rotating vortex was initially positioned under the airfoil symmetry plane at h/c = –0.2. One can observe that due to the vortex the flow patterns change more significantly for smaller core radius. This is revealed in a strong acoustic disturbance which can be noted for the reference core radius but not for the bigger one (see Figures 10b and d). The main part of the strong disturbance is displaced into the space below the airfoil. The explanation of this is based on the stagnation point behavior when the vortex approaches the airfoil. In the phase when the vortex is close to the leading edge the stagnation point is on the bottom surface of the airfoil. Its displacement down from the leading edge is larger for smaller core radius. The position of stagnation point when it is passed by the vortex shows the location of the source of the acoustic disturbance. The disturbance emerges due to the expansion of the air in the stagnation region which was previously compressed to high pressure owing to the vortex.

In Figure 11, the histories of C_l for four values of the vortex core radius are compared. One can note that the predicted amplitude of C_l for core radii considered are close to one another. This is due to the flow velocity at h/c = 0.2 induced by the vortex which changes in a relatively small domain for vortex radii in the range r_o–$5r_o$ (see Figure 8).

The acoustic wave during the airfoil-vortex interaction (compressibility wave

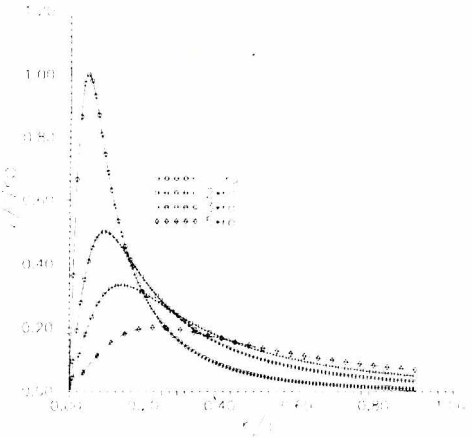

Figure 9. *Flow velocity distributions in the vortex for various core radius,* $\Gamma_0 = 50\ m^2/m$, $(v_q)_{r=r0} = 147$ m/s, $r_o = 5.4$mm

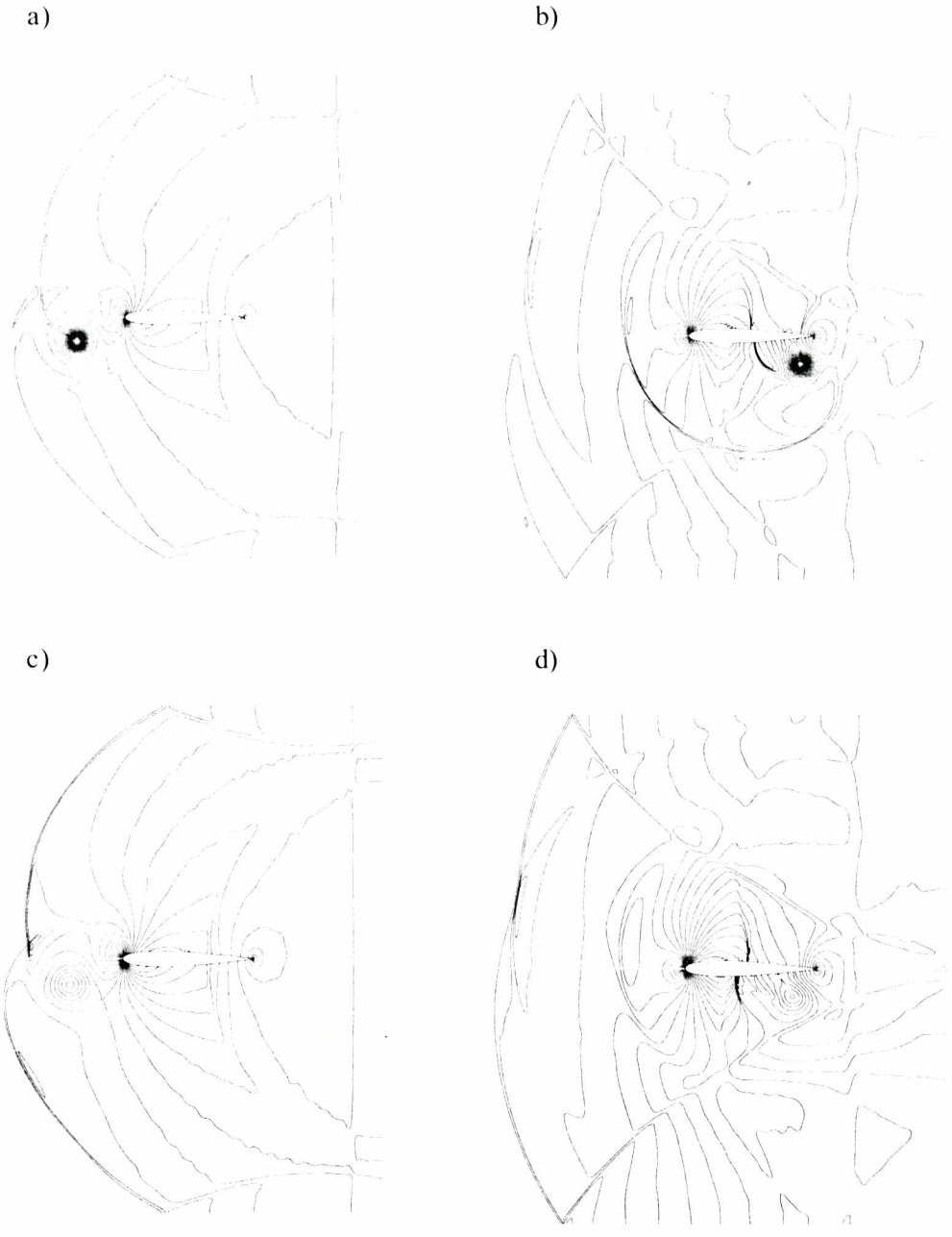

Figure 10. *Flow patterns during the vortex passage for core radius* r_o *(first column) and* $3r_o$ *(second column). Delay in relation to the moment when the incident shock wave reaches the leading edge: (a, c) 0.678 ms, (b, d) 1.186 ms*

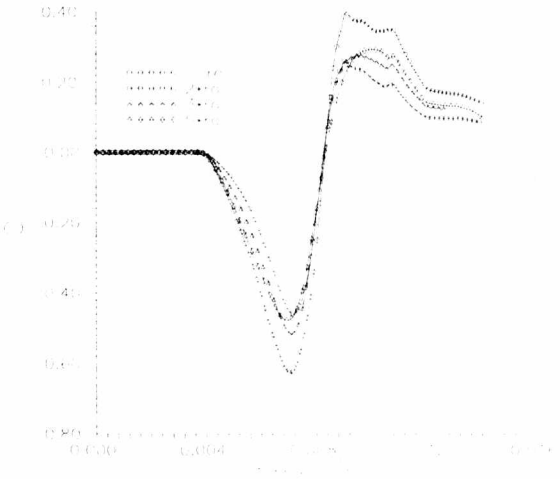

Figure 11. *Lift coefficient variations for various core radius*

[7]) is illustrated in Figure 12. It shows the instantaneous (for the time instants 0.508, 0.678, 0.848, 1.017, 1.186 and 1.355 ms) pressure distributions along the line passing through the leading edge at –135 deg to the flow velocity vector at infinity. One can note that for the reference case the acoustic wave forms a shock wave which weakens during its motion. It is not the case for a large core radius ($5r_o$). Now, the acoustic wave presents a continuous relatively small increase of the pressure. This can be observed on the pressure distributions (Figure 13) along the line mentioned above for the core radii considered.

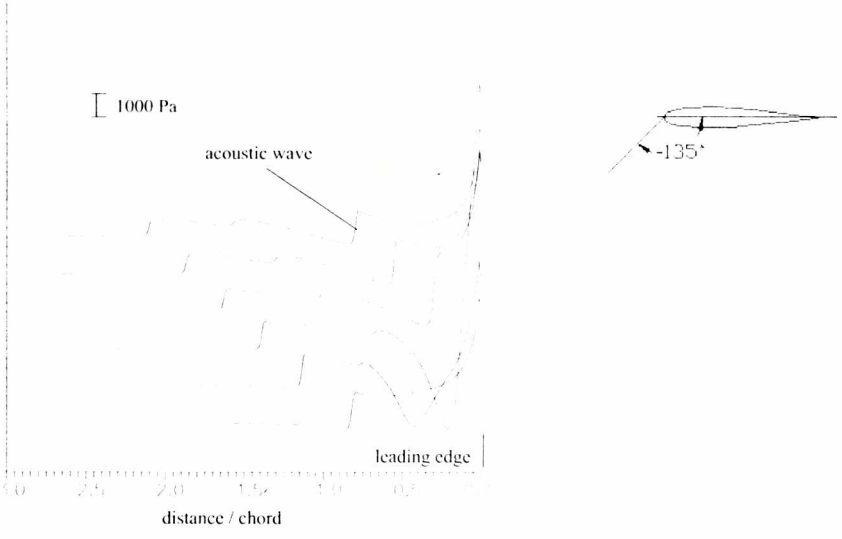

Figure 12. *Instantaneous pressure distributions along the line passing through the leading edge at –135 deg to the flow velocity vector at infinity corresponding to flow patterns in Figure 10*

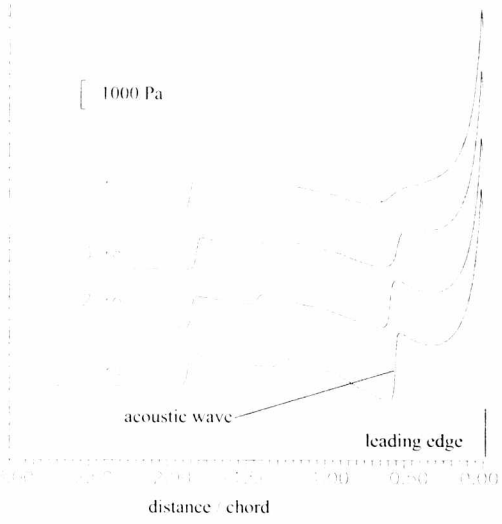

Figure 13. *Instantaneous pressure distributions like in Figure 12 at the instant t = 1.355 for various core radii of the vortex*

6. Conclusions

Vortex trajectory appears to be an important parameter controlling the airfoil-vortex interaction. The effects of the AVI are much stronger when the vortex approaching to the airfoil accelerates the flow at the pressure surface of the airfoil than in the case when the vortex decelerates the flow at the suction surface. These cases correspond to the clockwise rotating vortex passing under or over the airfoil considered in the present studies, respectively. The miss distance strongly affects the instantaneous pressure distributions along the airfoil, which leads to strong variations of the lift coefficient.

Variations of the lift coefficient depend first of all on the flow velocity induced by the vortex close to the airfoil surface. If this velocity is constant for various vortex radii, the lift coefficient changes approximately in the same way. In contrast to this the strength of the acoustic wave and its direction strongly depend on the core radius even for a constant induced flow velocity. The acoustic wave is stronger for a smaller vortex core radius.

References

[1] Lee S. and Bershader D., *An Experimental and Computational Study of 2-D Parallel Blade - Vortex Interaction*, AIAA Paper 91-3277

[2] Lee S. and Bershader D., *Head - On Parallel Blade - Vortex Interaction*, AIAA Journal Vol 1. No 1. 1994, pp 16-22

[3] Damodaran M. and Caughey D., *Finite — Volume Computation of Inviscid Transonic Airfoil - Vortex Interaction*, AIAA Journal Vol 26, No 11, 1988, pp. 1346-1352

[4] Ehrienfried K., *Numerische Untersuchung von Wirbel-Tragflugel-Wechselwirkungen im transsonischen Geschwindigkeitbereich*, Max-Planck-Institut fuer Stroemungsforschung Report 8/1991

[5] Gallman J., *Parametric Computational Study of Isolated Blade-Vortex Interaction Noise*, AIAA Journal Vol 32, No2. 1994, pp. 232-238

[6] Szumowski A., Piechna J., Selerowicz W. and Sobieraj G., *Modified Formula for the Velocity Distribution in a Vortex*, AIAA Journal (to be published)

[7] Van Leer B., *Flux-Vector Splitting for the Euler Equations*, Lecture Notes in Physics. Vol. 170, 1982, pp 507-512

[8] Kamiński W. and Szumowski A., *Acoustic Effects of Parallel Vortex-Airfoil Interaction*, Journal of Sound and Vibration, 1995, 183(2) pp. 209-220